Catalysis Communications 183 (2023) 106767

Contents lists available at ScienceDirect

Catalysis Communications

journal homepage: www.elsevier.com/locate/catcom

Heterogeneous photo-Fenton process with zerovalent iron nanoparticles for degradation of toluene in aqueous solution

Clara Duca [a,b,1], Horacio Bogo [a,b], Marta I. Litter [c,*], Enrique San Román [a,b,2]

[a] Instituto de Química Física de los Materiales, Medio Ambiente y Energía (UBA – CONICET), Facultad de Ciencias Exactas y Naturales, Ciudad Universitaria, Pabellón 2, 1428 Ciudad Autónoma de Buenos Aires, Argentina

[b] Departamento de Química Inorgánica, Analítica y Química Física (FCEN – UBA) Facultad de Ciencias Exactas y Naturales, Ciudad Universitaria, Pabellón 2, 1428 Ciudad Autónoma de Buenos Aires, Argentina

[c] Escuela de Habitat y Sostenibilidad, Universidad Nacional de Gral, 25 de Mayo y Francia, 1650 San Martín, Prov. de Buenos Aires, Argentina

ARTICLE INFO

Keywords:
Toluene
Zerovalent iron nanoparticles
Heterogeneous Fenton
Heterogeneous photo-Fenton

ABSTRACT

Degradation of toluene by treatment with zerovalent iron nanoparticles and different H_2O_2 concentrations under UVA light has been analyzed at pH 3. The highest removal of toluene was found with 100 mg L^{-1} nZVI and 400 mg L^{-1} H_2O_2, but 100 and 200 mg L^{-1} of H_2O_2 were used in most experiments as the degradation rate was similar. Experiments with Fe(II) (10 and 1 mg L^{-1}) were performed for comparison. Benzaldehyde and bibenzyl were found the main oxidation products. nZVI could be reused without loss of efficiency. A mechanism was proposed.

1. Introduction

Wastewater produced by petroleum refineries contains aliphatic and aromatic petroleum hydrocarbons, such as hydrocarbons, benzene, toluene, ethylbenzene, xylene, polynuclear and polycyclic aromatic hydrocarbons, long-chain hydrocarbons, and nitrogenous heterocyclic compounds. These substances provoke harmful and hazardous impacts on surface and groundwater sources, crop production, living organisms, and human health [1]. Specifically, gasoline is a complex mixture of organic compounds, mainly hydrocarbons, from which aromatic compounds constitute an especially relevant fraction [2]. Aromatic compounds are predominant in the water-soluble portion of gasoline, and benzene, toluene, ethylbenzene, and xylenes (BTEX) form the bulk of the total dissolved components, and pH values between 4.3 and 10 were reported [3].

However, the aromatic hydrocarbons cannot be degraded adequately by conventional treatment methods as most of them only transfer the pollutant from one media to another [1,4]. Therefore, other technologies should be considered to remove the aromatic water-soluble fraction. In this sense, advanced oxidation processes (AOPs), based on the production of very reactive and highly unselective species (especially hydroxyl radicals, $HO^{\bullet}$), can be used for the treatment of refractory compounds and are promising technologies to improve the efficiency of petrochemical wastewater treatment [3]. Among them, Fenton and photo-Fenton oxidation are low-cost and effective methods for organic contamination removal, and several reviews have been published in the last years (e.g., [5–8] and references therein).

The complete mechanism of the Fenton process is still under intense and controversial discussion, but it is accepted that iron cycles continuously between Fe(II) and Fe(III) [8,9]. The basic reaction scheme for Fenton processes is indicated in Appendix A (Eqs. (A1)–(A22)) where $HO^{\bullet}$ and FeO^{2+} are proposed as oxidizing species for organic compounds [5,6,8,9]. $HO^{\bullet}$ are very powerful reactive oxygen species (ROS), with a standard redox potential of 2.73 V vs. SHE and low selectivity for the attack to chemical species [10]. The participation of FeO^{2+} is still under discussion [11,12].

For the treatment of petrochemical wastewater, groundwater of petroleum gas stations, synthetic and real groundwater oil refinery wastewater contaminated with gasoline, diesel treatment, etc., Fenton and photo-Fenton processes have been proposed and some reviews have been published (e.g., [13]). Coelho et al. [14] found that these AOPs were the most effective to remove the organic matter of petroleum refinery sour water. Optimization of a photo-Fenton oxidation process for polycyclic aromatic hydrocarbons degradation from potable water was

* Corresponding author.
E-mail address: mlitter@unsam.edu.ar (M.I. Litter).
1 Present address: Department of Industrial Chemistry "Toso Montanari", University of Bologna, Italy

2 Deceased. This work is dedicated with immense gratitude to his memory as he initiated the research.

https://doi.org/10.1016/j.catcom.2023.106767
Received 9 September 2023; Accepted 14 September 2023
Available online 16 September 2023

also achieved [15]. Treatment of BTEX (benzene, toluene, ethylbenzene, and xylene) mixtures by Fenton and photo-Fenton based reactions have been reported [4,16].

In recent times, solid iron-containing catalysts such as zerovalent iron (micro- or nanoparticulate), iron oxides and oxyhydroxides (Fe_2O_3, Fe_3O_4, goethite), Fe^0/Fe_3O_4, iron-immobilized materials, etc., have been proposed to be used in heterogeneous Fenton processes (e.g., [8,17–19] and references therein). Use of nanoparticles (nZVI) improves the heterogeneous Fenton technology performed with Fe(0) microparticles, due especially to the large surface area to volume ratio of the particles and their enhanced reactivity [20,21]. A detailed mechanism of this Fenton-like process with nZVI is indicated in the Appendix A (Eqs. (A23)–(A38)) and it is similar to that occurring during the corrosion of other types of metallic iron (e.g., [22] and references therein). Briefly, in the presence of water or water and dissolved oxygen, the iron nanoparticles are oxidized, and the process involves the participation of Fe species in different oxidation states. Fe^0 is oxidized to Fe^{2+}, giving water or hydrogen peroxide as the main products. The formation of Fe^{2+} and H_2O_2 (Fenton reaction [8]) on the corroded Fe^0 surface gives $HO^\bullet$, which causes the oxidation of Fe^{2+} to Fe^{3+}. Fe^{3+} can be reduced again to Fe^{2+} by a second H_2O_2 molecule, giving the perhydroxyl radical ($HO_2^\bullet$). This radical can also reduce Fe^{3+} to Fe^{2+}, and this is a key step to maintain the production of $HO^\bullet$. Then, Fe^{2+} reacts to give oxides and oxyhydroxides (FeOx) such as magnetite (Fe_3O_4), maghemite (γ-Fe_2O_3), lepidocrocite (δ-FeOOH), ferrous hydroxide ($Fe(OH)_2$), or ferric hydroxide ($Fe(OH)_3$), depending on the redox conditions and pH (e.g. [23]). The corrosion of Fe^0 generates, in addition, reactive oxygen species (ROS) such as superoxide, $HO_2^\bullet$, H_2O_2, etc., able to oxidize and remove the compounds. Thus, oxidation of pollutants may potentially occur via iron ions released into solution or reactions that take place between solutes and surface-bound species. Then, the course of reactions would follow the typical Fenton mechanisms to yield oxidized products or the total mineralization of the organic compound [9]. Other possible reactions taking place during the photo-Fenton processes with nZVI can be the action of FeOx as photocatalysts, which will be explained in Section 3.8. As an example, low-cost goethite recovered from acid mine drainage was applied to the treatment of a simulated petrochemical wastewater in a photo-Fenton process [19].

In the case of toluene, homogeneous Fenton reactions have been described many years ago, by e.g., Merz and Waters in 1949 [24], who indicated that the treatment with Fe^{2+} and H_2O_2 at very acid pH (ca. 1) transformed the compound into a mixture of bibenzyl, benzaldehyde, and cresols, suggesting an attack by free $HO^\bullet$ both in the side chain and in the nucleus. Walling and Johnson [25] indicated that the products of the Fenton reaction of aromatic compounds, including toluene, started by the formation of hydroxycyclohexadienyl radicals by $HO^\bullet$ addition to the aromatic system. Huling et al. [26] reported a highly efficient toluene transformation initiated by Fenton-like reactions, proposing a mechanism for this reaction.

Fenton or photo-Fenton processes with nZVI were proven to be effective to treat petroleum aromatic hydrocarbons (PAHs), TPH, and BTEX components [27]. However, to the best of our knowledge, no examples on the treatment of single aromatic pollutants with nZVI in Fenton processes with a mechanistic approach are found in the literature.

In this work, the degradation of toluene, selected as a prototypical pollutant, in aqueous solution, applying a heterogeneous photo-Fenton process based on nZVI has been studied, using different iron and H_2O_2 concentrations. Some results in the dark are also presented. A comparison with homogeneous Fenton processes using Fe(II) in water solution is included.

2. Experimental section

2.1. Materials and chemicals

NANOFER Star (NSTAR) was provided by NANOIRON, s.r.o. (Czech Republic). Toluene (99.5%), hexane (pure grade) and diethylether (98%, containing butylated hydroxytoluene (BHT) as stabilizer) were Sintorgan. Fe(II) as Mohr's salt ($Fe(NH_4)_2(SO_4)_2{\cdot}6H_2O$) was ACS reagent ($\geq$ 99%), hydrogen peroxide 30% was Riedel de Haën, and $KMnO_4$ (90–98%) was Mallinckrodt. Iron (III) perchlorate hydrate ($Fe(ClO_4)_3{\cdot}H_2O$, 98%), benzaldehyde (reagent plus >99%), benzyl alcohol (99.89%), bibenzyl (1,1′-(ethane-1,2-diyl)dibenzene or 1,2-diphenylethane, 99%), ammonium iron(II) sulfate hexahydrate ($Fe(NH_4)_2(SO_4)_2.6H_2O$), sodium fluoride (NaF, 99%), *o*-phenanthroline (99%), and ammonium acetate (CH_3COONH_4, reagent grade) were Sigma Aldrich. Anhydrous sodium sulfate (Na_2SO_4, 99%) and H_2SO_4 (95–98%) were Merck. *o*-Cresol (puriss. p.a. standard for GC) was Fluka, *p*-cresol (extra pure) was Anedra, and dipotassium oxalate monohydrate ($K_2C_2O_4.H_2O$, for analysis) was Timper. All other reagents were of the highest available purity.

All solutions and suspensions were prepared with Milli-Q (Millipore) (resistivity = 18 MΩ.cm). For pH adjustments, H_2SO_4 diluted to 1:5 *v*/v was used.

2.2. Toluene oxidation experiments

Batch experiments were carried out in a cylindrical jacketed Pyrex glass reactor with an internal diameter of 5.3 cm and a height of 13 cm filled up to 310 mL and sealed during all the experiments with a rubber stopper lined with a polystyrene film in order to avoid contamination of the water. The temperature was controlled by a water bath circulator heater (HAAKE N3) kept at 25 °C by a cooler circulator (Julabo MH). For experiments under UVA light irradiation, a CLEO HPA 400/300 SD ozone free lamp (λ_{em} = 300–400 nm, output power = 400 W), was used. Fig. A1 (Appendix A, Section A2) shows the main setup components.

A toluene mother solution was prepared by placing 20 mL toluene in contact with 200 mL water in a separation funnel. After vigorous stirring and decanting, the organic phase was discarded, and 400 mL of water were added. The concentration of toluene in the water phase was measured by GC–MS and was approximately 100 mg L^{-1}. This solution was diluted in order to obtain the desired toluene concentrations and added to the cylindrical reactor. Weighed amounts of nanoparticles, used as received, were suspended in 2 mL water, and sonicated for 5 min using a Testlab ultrasonic cleaner. The suspension was poured into the reactor containing the toluene solution with additional 4 mL water. Nanoparticle concentrations used were alternatively 10 or 100 mg L^{-1}. The reactions were made at pH 3, and a slight increase of pH up to 3.15 in 30 min was observed. Experiments were performed in the dark and under UVA irradiation. Additional experiments were performed at pH 4 and 5.

To quantify the adsorption of toluene on the nanoparticles, 10 mL of the toluene mother solution were put in contact with 1 g of NSTAR for 60 min in the dark at pH 3. The suspension was centrifuged at 3500 rpm with a Presva DCV-16RTV centrifuge, and the nanoparticles were separated. The toluene solution was extracted with 1.5 mL hexane, the used nanoparticles were washed 3 times with 3 mL water, and the water solution was extracted again with 1.5 mL hexane.

For homogeneous Fenton and photo-Fenton experiments, Fe(II) as Mohr's salt (60 or 600 mg) was dissolved in 50 mL water, and 2 mL of the solution were added to the reactor in order to obtain an initial concentration of 1 or 10 mg L^{-1} of Fe(II) (equivalent to 0.18 and 1.8 mM Fe(II), respectively). The same protocol as with the solid nanoparticles was followed.

For Fenton experiments, H_2O_2 30% in different amounts in order to reach concentrations in the 25–600 mg L^{-1} range was added at once with a syringe through a PTFE catheter (Fig. A1), after closing the

reactor and beginning the stirring.

All experiments lasted 30 min. In each experiment, 3 mL of the reaction mixture were sampled through the catheter every 5 min, extracted with 1.5 mL hexane after vigorous stirring, and centrifuged for 5 min at 13000 rpm. Finally, 1 mL of the hexane solution was transferred to a vial for toluene analysis (see Section 2.3). At the end of the experiments, the reaction mixture was centrifuged in 50 mL vials in order to separate the remaining nanoparticles or solid oxides produced during the treatment. Finally, 25 mL of the liquid phase were separated to measure the final H_2O_2 concentration, 12 mL to measure the concentrations of Fe(II) and total iron (Fe_T) in solution, and the remaining volume was used to quantify the remaining toluene and oxidation products by GC–MS. The separated particles were dried under vacuum and characterized by X-ray diffraction (XRD) spectroscopy (see section 2.3).

Blank experiments were performed in the absence of H_2O_2 and iron (NSTAR or dissolved Fe(II)), with and without UVA light, to verify that the toluene concentration did not decay by evaporation or leakage through the reactor closing setup.

Experiments at pH 4 and 5 were performed similarly and no pH changes were observed at the end of the experiments.

One experiment under UV light was carried out with 100 mg L^{-1} toluene at pH 3 in the presence of 100 mg L^{-1} H_2O_2 and 10 mg L^{-1} of nanoparticles to test the reuse of the nanoparticles. In this case, after the reaction, the nanoparticles were separated, dried, and used for a second time under the same conditions indicated above. The solid (3 mg) was suspended in 2 mL water, sonicated for 5 min, and the suspension was poured into the reactor containing a fresh toluene (100 mg L^{-1}) solution and 100 mg L^{-1} H_2O_2, with additional 4 mL water. The remaining toluene was measured after 30 min of reaction in both cases.

2.3. Analytical methods

Toluene was analyzed by CG-MS, calibrating with a standard each day. For this determination, 1 μL of the hexane extract of each experiment was injected into the gas chromatograph (Agilent Technologies 7890 A) fitted with a 30 m long, 0.25 mm diameter and 0.25 μm film thickness HP-5MS column, coupled to a triple-axis mass detector (Agilent Technologies 5975C). Operational conditions were as follows: carrier gas, helium at 1.5 mL min^{-1}; injection mode, split 10:1; injector and detector temperature, 300 and 250 °C, respectively; temperature program, 5 min at 50 °C followed by a ramp at 17 °C min^{-1} up to 250 °C. The total run time was 16.7 min. Toluene standards (200 mg L^{-1}) were prepared in hexane and injected before each run. Chromatographic runs were short, about 5 min.

Reaction products were analyzed by GC–MS under the same conditions as toluene on the remaining volume of the final reaction mixture. In the experiments to measure the products, the decay of the toluene concentration was followed withdrawing aliquots of 2.5 mL each 5 min as indicated before but in longer runs (60 min). After the withdrawal of all the samples for the toluene analysis from the reactor, the rest of the volume (approx. 295 mL) was poured together with 50 mL of diethylether in a separation funnel. Then, 20 mL of the organic phase were put in contact with 3 g anhydrous sodium sulfate in order to extract water. The solvent (diethylether) was evaporated under an argon stream by heating in a water bath at ca. 35 °C to obtain a final volume of 1 mL, 1 μL of which was injected into the GC–MS equipment. To obtain a relative calibration, peak areas were compared with that of BHT, the ether stabilizer contained in the used solvent (see section 2.1), as a quasi-internal standard.

The products analyzed were benzaldehyde, benzyl alcohol, *o*-cresol, *p*-cresol, and bibenzyl. These compounds were selected based on the intensity of the signal compared with other reaction products for those assuring a matching above 95% between the NIST 11 library of the chromatograph and the experimental spectrum. The extraction yield of the different reaction products was obtained from standards of the pure compounds extracted in the same conditions as the samples. 2,2'-Dimethylbiphenyl, benzyltoluene, and biphenyl were also identified by the NIST library; however, as they were formed at very low concentrations, they were not quantified.

To calculate the final H_2O_2 concentration, 25 mL of the reaction mixture were acidified with 10 mL of a solution 1:5 *v*/v of concentrated H_2SO_4 and titrated with 0.1 N $KMnO_4$. The final concentrations of Fe(II) and Fe_T (total iron, i.e., Fe(II) + Fe(III)) in solution were measured spectrophotometrically at 508 nm using the *o*-phenanthroline method [28]. The concentration of Fe_T was determined by adding to the sample 0.2 mL of hydroquinone 1% *w/v* to reduce Fe(III) to Fe(II) and measuring the sample as before. The Fe(III) concentration was calculated by subtracting the Fe(II) concentration from the Fe_T concentration. The content of Fe(0) in the NSTAR nanoparticles was determined by a modification of the method reported in [29], digesting a known amount of the powder in 0.5 N H_2SO_4, measuring the volume of H_2 formed, and determining the content of Fe_T, as described before.

XRD patterns were obtained using an Empyrean Range (Malvern Pananalytical) diffractometer with PIXcel 3D detector, using Cu-Kα radiation, over a 2θ range of 10–100° with a step size of 0.026° and a scan speed of 24 s per step.

The incident photon flux per unit volume ($q^\circ_{n,p}/V$) of the lamp was determined through potassium ferrioxalate actinometry. A 0.015 M potassium ferrioxalate solution was prepared inside the reactor mixing two equal parts of 0.030 M ammonium Fe(III) sulfate solution with 0.090 M dipotassium oxalate in 0.1 N H_2SO_4. The lamp of the reactor was turned on, left to stabilize for 2 min, and 0.2 mL of the irradiated solution was taken every 20 s during 3 min reaction time. The Fe concentration was spectrophotometrically measured by the *o*-phenantroline method at 508 nm. The determined $q^\circ_{n,p}/V$ was 82.5 μeinstein s^{-1} L^{-1}.

3. Results and discussion

3.1. Use of NANOFER Star

NANOFER STAR is dry air-stable nZVI powder, where the surface of iron nanoparticles is stabilized by a thin layer of iron oxide, preventing immediate oxidation in contact with atmospheric oxygen. According to the manufacturers [30], commercial NSTAR iron nanoparticles are composed of ≥65–80% Fe(0) and 35–20% of iron oxides, with a specific surface area of ≈ 20 m^2 g^{-1}. This material can be easily and safely stored, transported, handled, and processed compared with non-stabilized nZVI, and presents high reactivity [30]. According to the XRD pattern (see Fig. 6 below), the material presents the α-Fe phase, with other minor signals that could be assigned to iron oxides. These signals were assigned later to magnetite by Mössbauer spectroscopy, together with a complete characterization of the material that will be published elsewhere [31].

3.2. Blank experiments and adsorption of toluene on nZVI

No changes on the toluene concentration were observed after 60 min when introducing in the reactor 100 mg L^{-1} (1.1×10^{-3} M) toluene at pH 3 in the absence of H_2O_2 and iron (nZVI or Fe(II)), either in the dark or under UVA irradiation. This means that no reaction took place, that toluene did not evaporate to a detectable extent, and that the reactor was correctly sealed without losses due to a gas-phase toluene leak.

Experiments with toluene under the same initial conditions in

contact with nZVI (100 mg L^{-1}, ca. 1.25×10^{-3} M Fe, calculated based on a 70% content of Fe(0) in the original NSTAR nanoparticles, determined as indicated in section 2.3) were performed (absence of H_2O_2) to assess the adsorption of the compound onto the iron nanoparticles. The concentration of nZVI was 10 times higher than those used later in the Fenton and photo-Fenton reactions (sections 3.3 and 3.4) to allow a good recording of the results. After 60 min, there were no changes on the initial toluene concentration and no toluene was detected after separating through centrifugation and washing the nanoparticles with hexane, indicating that the adsorption of toluene on nZVI was not significant under these conditions.

The use of nZVI in the absence of H_2O_2 in removing benzene, toluene, ethyl benzene and xylene (BTEX) from aqueous solutions under different conditions was reported recently [32]. The authors obtained good results but higher nZVI doses than those used in the present work were used.

3.3. Fenton reaction

Experiments with 100 mg L^{-1} toluene, 100 mg L^{-1} nZVI, or 10 mg L^{-1} Fe(II) (1.8×10^{-4} M) together with 200 mg L^{-1} (5.8×10^{-3} M) of H_2O_2 were performed in the dark at pH 3 for 30 min. The H_2O_2 concentration was chosen because it was in the middle of the range (25–400 mg L^{-1}) used later in the photo-Fenton experiments (section 3.4). As said in section 2.2, only a slight increase of pH to 3.15 at the end of the experiment was observed. Temporal profiles of the normalized toluene concentration (C/C_0) (Fig. 1) show a slow degradation, <30%, without differences between the experiments with Fe(II) or nZVI. In both cases, approximately 70 mg L^{-1} of toluene remained in the solution.

Both curves could be fitted rather well to an exponential decay with good adjustment according to the correlation coefficients (R^2) and similar values of the pseudo-first-order rate constants (k) (Table 1). These results indicate that the amount and nature of the iron species did not play any significant role in this case.

3.4. Photo-Fenton reaction

Experiments (30 min duration) under UVA light with 100 mg L^{-1} toluene, H_2O_2 and nZVI or Fe(II) were performed. nZVI (100 and 10 mg L^{-1}) or Fe(II) (1 and 10 mg L^{-1}) were used, and 400 mg L^{-1} (1.1×10^{-2} M) of H_2O_2 was added at once (Fig. 2). Experiments were carried out at

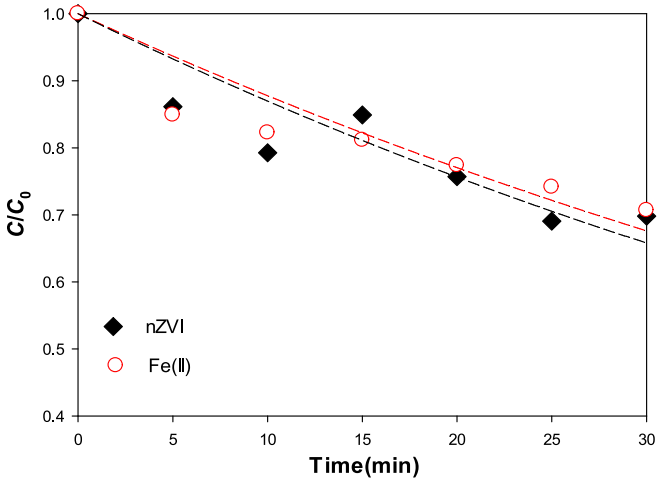

Fig. 1. Temporal profiles of the normalized toluene concentration (C/C_0) in the presence of nZVI or Fe(II) and H_2O_2 in the dark. Experimental conditions: 100 mg L^{-1} toluene, pH 3, 100 mg L^{-1} nZVI, or 10 mg L^{-1} Fe(II), 200 mg L^{-1} H_2O_2, T = 25 °C. Dashed lines are adjustments of the experimental points to an exponential fitting.

Table 1
Values of the percentage of degradation, pseudo-first-order rate constants (k) and correlation coefficients (R^2) values for toluene degradation extracted from Fig. 1.

Nature of iron	Iron concentration (mg L^{-1})	% toluene degradation	$k \times 10^2$ (min^{-1})	R^2
nZVI	100	30	1.40	0.796
Fe(II)	10	29	1.30	0.775

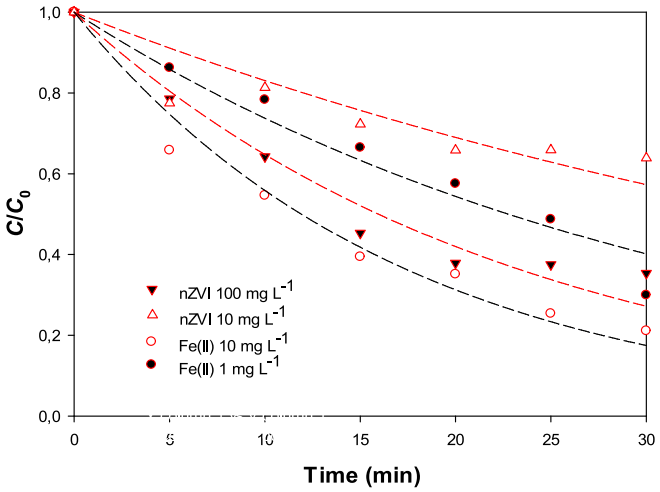

Fig. 2. Temporal profiles of the normalized toluene concentration (C/C_0) in the presence of nZVI or Fe(II) under UVA light and H_2O_2. Experimental conditions: 100 mg L^{-1} toluene, 10 or 100 mg L^{-1} nZVI, 10 mg L^{-1} Fe(II), 400 mg L^{-1} H_2O_2, T = 25 °C, $q^{\circ}_{n,p}/V$ = 82.5 μeinstein s^{-1} L^{-1}. Dashed lines are adjustments of the experimental points to exponential fittings.

pH 3; as said (section 2.2), a slight increase of pH to 3.15 in 30 min was observed in all cases.

The homogeneous reaction was faster than those with nZVI despite the amount of Fe was higher in all the heterogeneous reactions, as indicated by other authors (e.g., [19]). This can be explained because Fe added in the form of dissolved Fe(II) is more available for the reaction with toluene, while, in the case of the nanoparticles, Fe enters the solution in the form of Fe(0), and Fe(II) is generated by corrosion at acid pH, starting the photo-Fenton reaction at that point.

Fig. 2 also shows that toluene degradation increased with the amount of Fe used, either Fe(II) or nZVI, which is a common feature of Fenton processes and was observed for nZVI in the case of BTEX degradation [27], and in the treatment of TPH [1]. Although the adsorption of toluene on nZVI is low, as shown in Fig. 1 for the reaction in the dark, under irradiation, as soon as FeOx are formed (Eqs. (A28)–(A38)), new active sites are available, which increases the removal efficiency as the oxidation occurs on or near the surface of the iron particles [33–35]. Higher nZVI concentrations were not used in the present work because it has been reported that an excess can be detrimental, due to: 1) a possible filter effect caused by the nanoparticles, as reported in other cases [36,37] and 2) to the decomposition of H_2O_2 [1], as will be explained

Table 2
Values of the pseudo-first-order rate constants (k) and R^2 values for toluene degradation extracted from Fig. 2 (400 mg L^{-1} H_2O_2).

Nature of iron	Iron concentration (mg L^{-1})	% toluene degradation	$k \times 10^2$ (min^{-1})	R^2
nZVI	100	65	4.34	0.960
nZVI	10	36	1.85	0.728
Fe(II)	10	79	5.82	0.974
Fe(II)	1	70	3.04	0.956

below.

Toluene degradation followed a pseudo-first-order kinetic behavior, with good adjustment, irrespective of the initial concentration and nature of iron (nZVI or Fe(II)) and the amount of added H_2O_2. The same kinetics has been observed for BTEX degradation with nZVI [27]. Table 2 shows the values of the pseudo-first-order rate constants (k) and correlation coefficients (R^2) for toluene degradation using 400 mg L^{-1} H_2O_2 extracted from Fig. 2. The low value of R^2 for the experiment with 10 mg L^{-1} of nZVI can be due to experimental error.

Similar experiments were performed using different H_2O_2 concentrations (25–600 mg L^{-1}, i.e., 0.69 mM-0.020 M), and k values were extracted from plots similar to those of Fig. 2. Fig. 3 shows the variation of k using two different nZVI concentrations (100 and 10 mg L^{-1}) and two dissolved Fe(II) concentrations (10 and 1 mg L^{-1}).

In the case of nZVI at both concentrations (100 and 10 mg L^{-1}), an increase of k with the H_2O_2 concentration was observed up to around 100–200 mg L^{-1} H_2O_2, and then the rate remained almost constant (Fig. 3(a)). For Fe(II) at 10 mg L^{-1}, k increased constantly without reaching neither a maximum nor a saturation value. For Fe(II) at 1 mg L^{-1} the variation of k with the H_2O_2 concentration reached a maximum at around 200 mg L^{-1} H_2O_2, and then began to decrease (Fig. 3(b)); this last behavior probably takes place because Fe(II) is consumed and because of $HO^\bullet$ scavenging by an excess of the oxidant, both factors decreasing the rate.

Peroxide-to-iron molar ratios employed in Fenton treatments typically lie in the range 100 to 1000 [5]. Dehghani et al. [1], working on the removal of TPH (0.1–1 mg L^{-1}) with nZVI/UV/H_2O_2 indicated that H_2O_2 at concentrations higher than 5 mM acts as a scavenger of $HO^\bullet$, forming $HO_2^\bullet$ (Eq. (A6)), which has a lower oxidative ability than $HO^\bullet$. These authors indicate that the decomposition of H_2O_2 into oxygen and water (Eq. (A9)) has also a detrimental effect. Similar conclusions were extracted by Scaratti et al. [19]. Therefore, high concentrations of H_2O_2 inhibit the formation of $HO^\bullet$ and reduce the efficiency of the process. This agrees with the results here obtained when using nZVI, where concentrations of H_2O_2 higher than 100 mg L^{-1} stopped the reaction rate (Fig. 3(a)).

As similarly found for experiments of Fig. 2, the use of a higher iron concentration, either in the homogeneous or in the heterogeneous system, led to a higher toluene degradation rate. This can be explained because high Fe concentrations induce the formation of a higher amount of $HO^\bullet$, according to Eq. (A1). Similar results were found in the oxidation of PAHs using nZVI by a photo-Fenton process [27]. In the same study, the increase of the H_2O_2 concentration also improved the efficiencies of BTEX degradation, attributed again to a higher $HO^\bullet$ production. Higher H_2O_2 doses lead to scavenge $HO^\bullet$ through reaction of Eq. (A3), and the authors found that a molar Fe^0:H_2O_2 ratio of 0.3:1 was sufficient for BTEX removal (although the calculation was made considering that all Fe was Fe(0)).

Fig. 3 also showed that, with a H_2O_2 concentration lower than 100 mg L^{-1}, the degradation rate decreases, especially for the experiments with nZVI; therefore, H_2O_2 and, consequently, $HO^\bullet$ should be the limiting reagents. At a high Fe(II) and H_2O_2 concentrations, the reaction is arrested due to the consumption of $HO^\bullet$ (Eqs. (A3) and (A6)) [38].

Additionally, reactions between $HO^\bullet$ and toluene decomposition products and/or other scavengers (such as $HO_2^\bullet$ and $O_2^{\bullet-}$) would further reduce the transformation efficiency.

Fig. 4a and b show the variation of the percentage of toluene degraded as a function of the H_2O_2 consumed (measured as indicated in section 2.3) using nZVI and Fe(II) solutions and a 200 mg L^{-1} H_2O_2 concentration.

Fig. 4 indicates that when 100 mg L^{-1} nZVI and 1 mg L^{-1} Fe(II) are used, the initial 200 mg L^{-1} H_2O_2 concentration is enough to initiate the toluene degradation, with a good final toluene degradation. This is different for the other cases (10 mg L^{-1} nZVI and 10 mg L^{-1} Fe(II)), where a low toluene degradation or a high H_2O_2 consumption take place, due to a low amount of nZVI in the first case and an excessive amount of Fe(II) in the second case.

Table 3 shows the initial and final concentrations of Fe(II) and Fe_T in solution under the different conditions. The results indicate that some amount of Fe goes into solution at the end of the treatment, mainly as Fe (II). However, it is known that the toxicity of Fe in water is not very high concerning its incidence on human health, and there is no guideline value for iron in drinking water [39].

3.5. Reuse of the iron nanoparticles

Fig. 5 shows the results of experiments of toluene photodegradation (100 mg L^{-1}, pH 3) in the presence of 100 mg L^{-1} H_2O_2 and 10 mg L^{-1} of fresh and reused nanoparticles. After the first experiment, the solution was centrifuged to separate the nanoparticles, and the experiment was repeated using the separated nanoparticles and a fresh toluene solution at the same concentration and pH of the original experiment. However, it must be indicated that, in this case, the amount of nZVI was somewhat lower than that used in the initial experiment, since it was not possible to

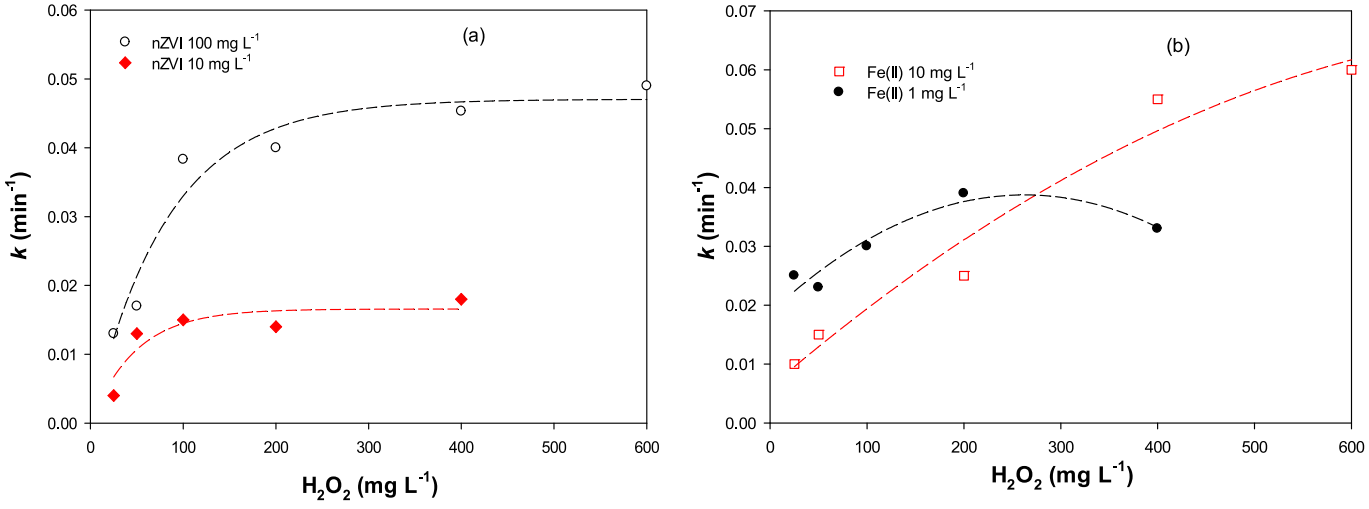

Fig. 3. Variation of the pseudo-first-order rate constants (k) in function of different H_2O_2 concentrations (25–600 mg L^{-1}) for the toluene photodegradation in the presence of (a) two nZVI concentrations (100 and 10 mg L^{-1}), and (b) two Fe(II) concentrations (10 and 1 mg L^{-1}). The k values were extracted from plots similar to those of Fig. 2 at the different H_2O_2 concentrations. Experimental conditions: 100 mg L^{-1} toluene, T = 25 °C, $q^\circ_{n,p}/V$ = 82.5 μeinstein s^{-1} L^{-1} and 30 min of reaction time.

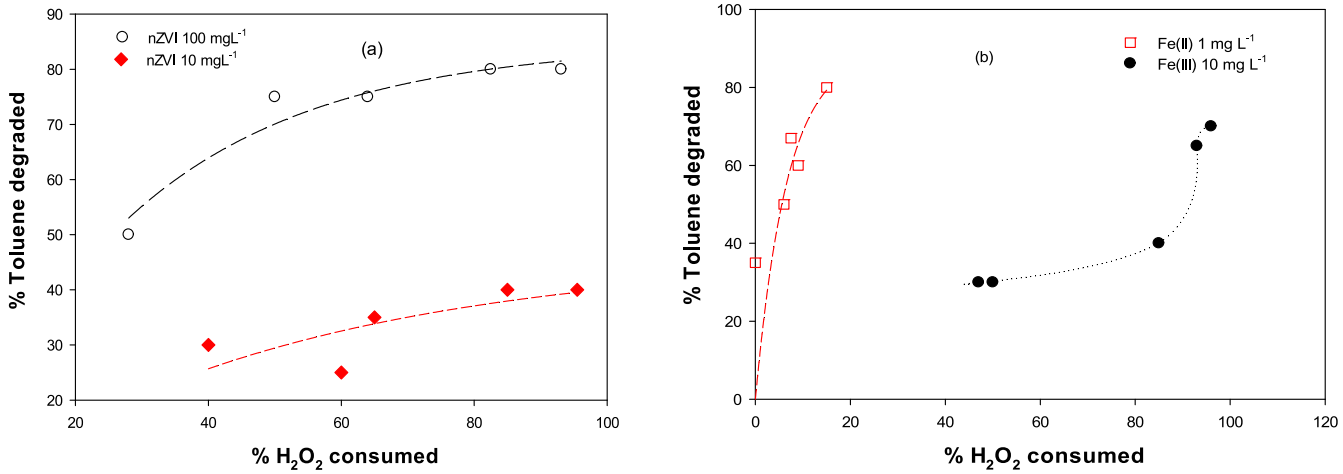

Fig. 4. Percentage of H_2O_2 consumed in function of toluene photodegraded at 30 min of reaction with (a) nZVI and (b) Fe(II). Conditions: pH 3, initial H_2O_2 concentration: 200 mg L^{-1}. The lines are only for visualization and do not correspond to any fitting equation.

Table 3
Initial and final (30 min reaction time) dissolved iron concentrations under different treatment conditions with nZVI or dissolved Fe(II). Toluene concentration: 100 mg L^{-1}, pH 3, H_2O_2 concentration: 200 mg L^{-1}.

Initial nZVI[a] or Fe(II) concentrations (mg L^{-1})	Fe_{Tdiss} (mg L^{-1})	Fe $(II)_{diss}$ (mg L^{-1})	Fe $(III)_{diss}$ (mg L^{-1})	% degraded toluene[b]
100 (nZVI)	9.4	8.6	0.8	70
10 (nZVI)	1.0	0.8	0.2	40
10 (Fe(II))	10.3	9.1	1.2	80
1 (Fe(II))	1.6	1.5	0.1	50

[a] Calculated on a 70% content of Fe(0) in the original NSTAR nanoparticles.
[b] The percentages of toluene degradation were different from those reported in Table 2 as the starting conditions were slightly different.

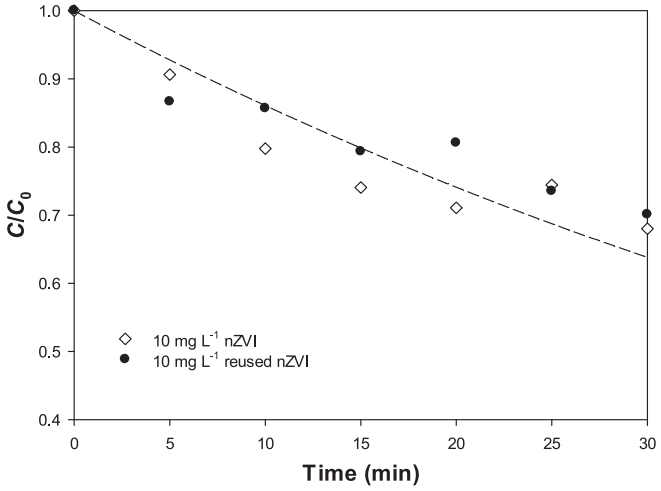

Fig. 5. Temporal profiles of normalized toluene concentration (C/C_0) in the presence of 10 mg L^{-1} fresh and reused nZVI and H_2O_2, at pH 3 under UVA light. Conditions: 100 mg L^{-1} (1.1×10^{-3} M) toluene, 10 mg L^{-1} nZVI (fresh and reused), 100 mg L^{-1} of H_2O_2 (2.94×10^{-3} M), $T = 25$ °C, $q^{\circ}_{n,p}/V = 82.5$ μeinstein s^{-1} L^{-1}. The dashed line is the adjustment of the experimental points to a pseudo-first-order kinetics, showing the same curve for both experiments.

separate the particles quantitatively after centrifugation as some of them remained attached to the walls of the centrifuge tubes. Nevertheless, the degradation degree of toluene was almost the same in both cases.

Thus, in contrast with the experiments with dissolved Fe(II), the nanoparticles can be recovered and reused, yielding a similar toluene degradation. This is an important advantage compared with the homogeneous system.

3.6. XRD patterns of the solid before and after the use of the iron nanoparticles

As said in section 2.2, after the experiments of toluene degradation under UVA light in the presence of nZVI and H_2O_2, the particles were separated and dried, and XRD patterns were taken and compared with that of the original nZVI particles. A typical diffraction pattern is shown in Fig. 6, where the solid obtained after an experiment of 100 mg L^{-1} toluene degradation under UVA light in the presence of 100 mg L^{-1} nZVI and 100 mg L^{-1} H_2O_2 was analyzed.

The XRD pattern indicates that the original material is essentially Fe (0) (with signals at $2\theta = 44.72$, 65.05, and 82.36 [40]) as indicated in section 3.1. A small contribution of iron oxides, such as magnetite or maghemite (that cannot be discriminated by this technique), is also observed ($2\theta = 35.5$). The XRD pattern of the solid obtained after UVA irradiation shows a decrease of the height of the Fe(0) peaks, suggesting that Fe(0) is consumed and oxidized to Fe(II), which then starts the Fenton process.

3.7. Products obtained during the processes

Tables 4–6 show the results of toluene degradation in the presence of nZVI and Fe(II) using different H_2O_2 concentrations at pH 3 after 30 min of reaction under UVA irradiation. Results of the normalized concentration of the main reaction products (percentage of each product divided by the percentage of BHT) at the final time, analyzed by GC–MS as indicated in section 2.3 are included. Tables 4–6 indicate the formation of several intermediates, and the incomplete mineralization of toluene. The main products were benzaldehyde and bibenzyl, with benzyl alcohol and both *o*- and *p*-cresols produced in minor amounts. It is important to remember that other products such as biphenyl, benzyltoluene and 2,2′-dimethylbiphenyl have been observed in the present work from GC/MS measurements but at very low concentrations and at long chromatographic run times (section 2.3). In almost all cases, the highest toluene removal results were obtained with 400 mg L^{-1} of H_2O_2.

Table 4 shows the results when 100 mg L^{-1} nZVI was used. It is observed that the degradation increased with the amount of H_2O_2, but

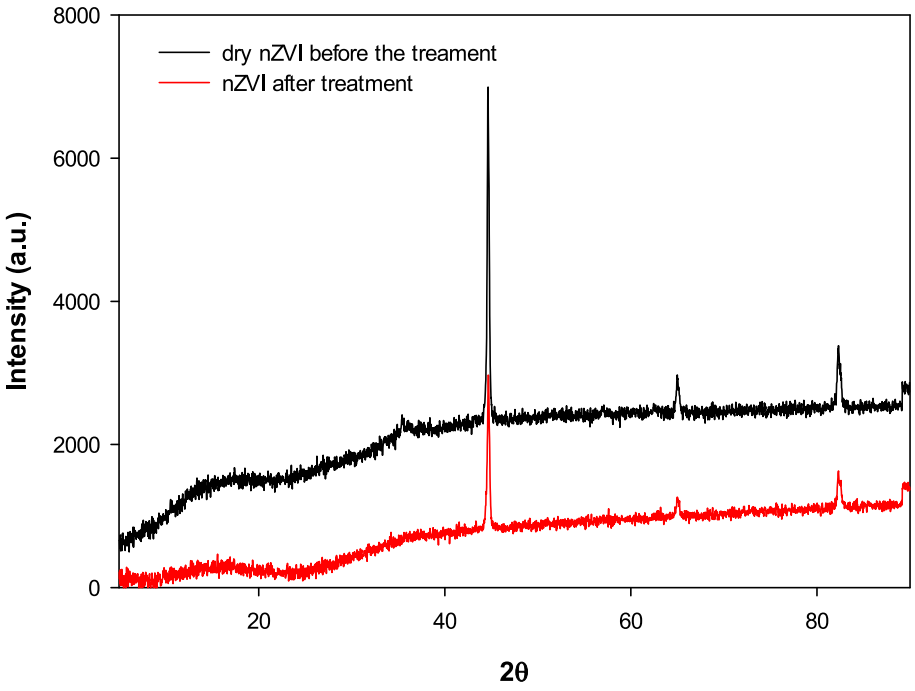

Fig. 6. X-ray diffraction patterns of the original nZVI and a dried sample of the solid obtained after the treatment of 100 mg L^{-1} toluene with 100 mg L^{-1} nZVI and 100 mg L^{-1} H_2O_2 under UVA irradiation, $T = 25$ °C, $q^{\circ}_{n,p}/V = 82.5$ μeinstein s^{-1} L^{-1}, pH 3 after 30 min of reaction time.

Table 4
Percentage of toluene degraded and normalized concentration of products (percentage of each product divided by the percentage of BHT) observed after 30 min of reaction of toluene (100 mg L^{-1}) in the presence of 100 mg L^{-1} nZVI and different H_2O_2 concentrations, pH 3 and $T = 25$ °C, under UVA irradiation.

[H_2O_2] (mg L^{-1})	% toluene degradation	benzaldehyde	bibenzyl	benzyl alcohol	*o*-cresol	*p*-cresol
25	32	0.5	0.1	0.0	0.1	0.2
50	29	0.7	0.4	0.0	0.2	0.2
200	40	0.8	2.0	0.1	0.2	0.2
400	82	0.7	2.4	0.1	0.1	0.2
600	71	0.8	3.8	0.2	0.2	0.2

Table 5
Percentage of toluene degraded and normalized concentration of products (percentage of each product divided by the percentage of BHT) observed after 30 min of reaction of toluene (100 mg L^{-1}) in the presence of 10 mg L^{-1} nZVI and different H_2O_2 concentrations, pH 3 and $T = 25$ °C under UVA irradiation.

[H_2O_2] (mg L^{-1})	% toluene degradation	benzaldehyde	bibenzyl	benzyl alcohol	*o*-cresol	*p*-cresol
25	14	0.1	0.0	0.0	0.1	0.2
50	29	0.5	0.1	0.1	0.2	0.2
100	32	0.6	0.2	0.1	0.2	0.3
200	35	0.6	0.2	0.2	0.2	0.3
400	37	0.4	0.0	0.1	0.2	0.3

Table 6
Percentage of toluene degraded and normalized concentration of products (percentage of each product divided by the percentage of BHT) observed after 30 min reaction of toluene (100 mg L^{-1}, pH 3) in the presence of 10 mg L^{-1} dissolved Fe(II) and different H_2O_2 concentrations under UVA irradiation.

[H_2O_2] (mg L^{-1})	% toluene degradation	benzaldehyde	bibenzyl	benzyl alcohol	*o*-cresol	*p*-cresol
25	24	0.6	1.1	0.2	0.1	0.2
50	70	0.6	1.1	0.2	0.1	0.2
100	89	0.8	1.0	0.3	0.1	0.2
200	90	1.2	0.5	0.5	0.2	0.2
400	79	1.3	0.0	0.5	0.2	0.2

the addition of 600 mg L^{-1} H_2O_2 was detrimental. Benzaldehyde production increased until 200 mg L^{-1} H_2O_2 was used, and then remained approximately constant. In contrast, bibenzyl grew monotonously with the amount of added H_2O_2. This can be explained because bibenzyl is formed from coupling of benzyl radicals, as will be explained in section 3.8; in the presence of nZVI, Fe(II) production is low, and more H_2O_2 is needed to form these radicals. As said, benzyl alcohol and the cresols were produced in minor amounts.

Table 5 shows the same results using an nZVI concentration ten times lower, where, as already seen in Fig. 2, the toluene degradation was much lower.

Again, the best results were obtained with 400 mg L^{-1} of H_2O_2. Benzaldehyde was here the main product and the amount of bibenzyl, benzyl alcohol and both cresols were minor and approximately constant.

Table 6 shows the percentage of toluene degraded and the concentration of products formed in the homogeneous Fenton reaction using 10 mg L^{-1} dissolved Fe(II). In this case, the toluene degradation was the highest when 100 and 200 mg L^{-1} H_2O_2 were added. The main products are benzaldehyde and bibenzyl, but the amount of this last product decreased when 200 mg L^{-1} H_2O_2 was used and negligible with 400 mg L^{-1} H_2O_2.

When 1 mg L^{-1} of Fe(II) was used (Table 7), the highest percentage of toluene degradation was obtained with 600 mg L^{-1} of H_2O_2. In this case, minor amounts of benzaldehyde were formed, and bibenzyl was the main product with an amount rather higher compared with the case of the experiments with 10 mg L^{-1} Fe(II), decreasing slightly with the increase of H_2O_2; the other products remained low and almost constant. In these cases, the amount of bibenzyl at low H_2O_2 concentrations is high because the bibenzyl radicals can react between them more easily. When H_2O_2 increases, bibenzyl decreases and almost disappears, while benzaldehyde increases.

Comparison of Tables 5 and 6, where similar amounts of iron were used, indicates that the concentration toluene remaining and of all byproducts was lower with nZVI and, especially, that of bibenzyl was very low.

Summarizing, the results of Tables 4–6 indicate that the removal of toluene increases with the amount of H_2O_2 although, in some cases (e.g., 600 mg L^{-1} in Table 4), a high amount is detrimental. The best results of the toluene heterogeneous degradation were found with 100 mg L^{-1} nZVI and 400 mg L^{-1} H_2O_2 (82% removal, Table 4). The homogeneous reactions produced higher amounts of bibenzyl. These results will be discussed in the next section.

3.8. Mechanistic pathways of toluene oxidation through the heterogeneous Fenton processes

A heterogeneous Fenton system can generate $HO^{\bullet}$ by two methods: the heterogeneous catalytic mechanism or the homogeneous Fenton reaction occurring through the iron leached from the solid catalyst [18]. Possible Fenton-like reactions are indicated by Eqs. (A1)–(A38) in the Appendix A, although the true mechanism is still under discussion.

Photocatalytic processes initiated by FeOx formed in the system or already present on the surface of the iron nanoparticles, acting as semiconductors, can also be proposed as mechanistic pathways, as described by Eqs. (1)–(8) [37,41,42].

$$FeOx + h\nu \rightarrow e_{BC}^{-} + h_{BV}^{+} \quad (1)$$

$$H_2O\ (HO^{-}) + h_{BV}^{+} \rightarrow HO^{\bullet}\ (+H^{+}) \quad (2)$$

$$O_2 + e_{BC}^{-}\ (+H^{+}) \rightarrow O_2^{\bullet-}\ (HO_2^{\bullet}) \quad (3)$$

$$O_2 + e_{BC}^{-} + H_2O_2 \rightarrow HO^{\bullet} + HO^{-} \quad (4)$$

$$Fe(III) + e_{BC}^{-} \rightarrow Fe(II) \quad (5)$$

$$Fe^0 + h_{BV}^{+} \rightarrow \rightarrow Fe(II) \quad (6)$$

$$\equiv Fe(III) + e_{BC}^{-} \rightarrow \equiv Fe(II) \quad (7)$$

$$\text{Aromatic compound} + h_{BV}^{+}\ (HO^{\bullet} + H^{+}) \rightarrow \text{oxidized compound}\ (+H_2O) \quad (8)$$

In this sense, several years ago, Fujihira et al. [43,44] studied the photocatalytic oxidation of toluene under aerobic conditions over TiO_2 and other semiconductors and attributed the oxidation to $HO^{\bullet}$ formed in the process. The products were benzaldehyde, cresols, and bibenzyl, same compounds obtained in the homogeneous photo-Fenton reaction of toluene depending on the conditions, as earlier proposed and described above by Merz and Waters [24]. If Fe^{2+} was added to the system studied by Fujihira et al. [43,44], the main products were benzaldehyde and *o*-cresol, with the yield of all products increasing with the addition of low Fe^{2+} concentrations; 50 mM Fe^{2+} and higher concentrations were detrimental, attributed to a short circuiting of the cycling continuous transformation of Fe^{2+} to Fe^{3+}. Regarding the use of iron-based semiconductors, Zhang et al. [45] found that pure cubic β-Fe_2O_3 could degrade some dyes and phenol as a catalyst in a photo-Fenton reaction and verified that $HO^{\bullet}$ was the active species in the process. Therefore, the heterogeneous photocatalysis over the FeOx present or formed in the present system can take place because all of them absorb below 450 nm [37,41,42] and can promote toluene oxidation under the present irradiation conditions, following the reactions described by Eqs. (1)–(8).

It is very well known that $HO^{\bullet}$ (produced in Fenton or radiolytic systems) attacks toluene and forms very rapidly the hydroxymethylcyclohexadienyl radical ($HMCD^{\bullet}$) [25,46] (Eq. (9), $k_1 = 3 \times 10^9$ M^{-1} s^{-1}) [47–49], which eliminates water to form the benzyl radical (Eq. (10), $k_2 = 1.1 \times 10^6$ M^{-1} s^{-1}) [48,50].

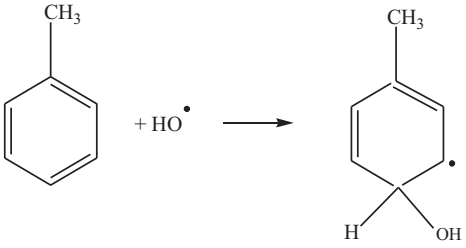

(9)

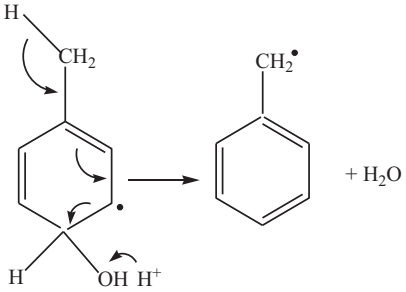

(10)

Table 7
Percentage of toluene degraded and normalized concentration of products (percentage of each product divided by the percentage of BHT) observed after 30 min reaction of toluene (100 mg L^{-1}, pH 3) in the presence of 1 mg L^{-1} dissolved Fe(II) and different H_2O_2 concentrations under UVA irradiation. The concentration of products is expressed as the percentage of each product divided by the percentage of BHT.

[H_2O_2] (mg L^{-1})	% toluene degradation	benzaldehyde	bibenzyl	benzyl alcohol	*o*-cresol	*p*-cresol
50	49	0.8	6.9	0.3	0.2	0.2
200	59	0.8	3.6	0.1	0.2	0.2
400	66	0.6	4.3	0.1	0.1	0.1
600	70	0.6	4.7	1.1	0.1	0.1

Bibenzyl is formed by the combination of two benzyl radicals (Eq. (11) [48]), explaining the increase in the production of this compound shown in Table 4:

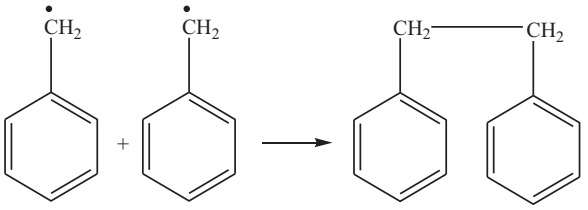

(11)

Huling et al. [26] confirmed the formation of the benzyl intermediate in the Fenton-like transformation of toluene with the formation of benzyl alcohol, cresols (the *ortho* form being the main product), benzaldehyde and benzoic acid byproducts (Eq. (12)).

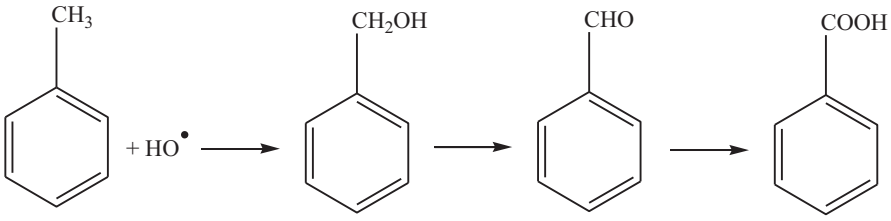

(12)

In oxygenated solutions, reaction of O_2 with HMCD$^{\bullet}$ competes favorably with the elimination of water from the radical, forming cresols (Eq. (13)):

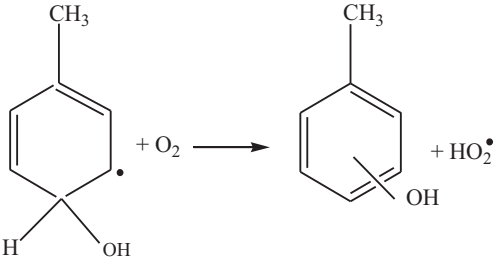

(13)

Benzyl alcohol and benzaldehyde are also formed from the benzyl radical, according to Eq. (14), although Walling and Johnson [25] suggested that the direct side-chain attack would be only a minor reaction path.

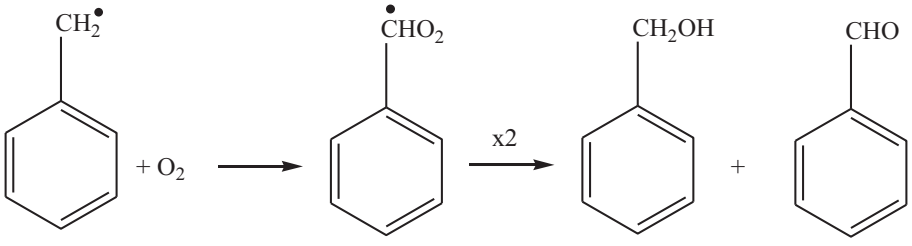

(14)

All these products and others such as *o*-hydroxybenzaldehyde, diphenylmethane, and 2,2′-bitolyl have been found before [25,26,44,50–53].

Xue et al. [16] say that, besides HO$^{\bullet}$, some other generated intermediate radicals (e.g., $C_6^{\bullet}H_6OH$, $C_6H_5^{\bullet}$, $C_6H_5^{\bullet}CH_2$) can couple, giving, for example, biphenyl, benzyltoluene, dimethyl biphenyl and others. As said (section 3.7), all these products have been observed in the present work but at very low concentrations and long chromatographic run times. According also to Xue et al. [16], the radicals can be scavenged by O_2, forming substitution and addition products, such as benzyl-*p*-cresol and 3-methylbenzophenone. HO$^{\bullet}$ attack towards benzene-ring could abstract H to form various intermediate phenols by disproportionation.

A very important point is that benzyl radicals are not expected to be formed largely at pH 3, as they are formed only in strongly acidic solutions by water elimination from HMCD$^{\bullet}$ through reaction of Eq. (15) [53]. For this reason, other sources of benzyl radicals have to be proposed. A possible oxidant fulfilling these conditions is $HO_2^{\bullet}$, the conjugate cation of $O_2^{\bullet-}$ formed in reactions (3), (A2), (A6), and (A20), which can react with toluene giving benzyl radicals (Eq. (15)):

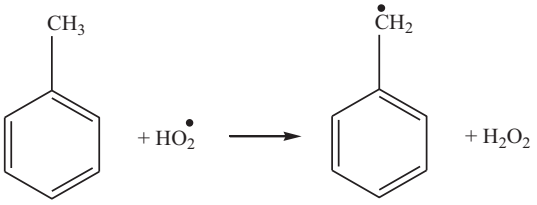

(15)

However, this reaction is extremely slow at room temperature [54]. Smith and Norman [51] indicate that $HO_2^{\bullet}$ is not the attacking species in Fenton reactions on toluene, probably because it is rapidly destroyed by further oxidation by Fe^{3+} (Eq. (A4)) or because it is much less reactive than HO$^{\bullet}$. In agreement, Choi et al. [55] indicate that, in the reductive degradation of toluene in the gas-phase in a pyrite Fenton system, the effect of $O_2^{\bullet-}$ was not significant and HO$^{\bullet}$ was identified as the dominant produced oxidant.

3.9. Role of pH

At pH 4 and 5, toluene photodegradation in the presence of nZVI did

not take place to a measurable extent under any of the conditions of the present work (results not shown).

As known, pH is one of the most important factors on the performance of Fenton-like processes (e.g., [5,56]). A similar effect can be expected when nZVI is used, as, for example, the Fe(0) corrosion rate is high at pH 2, decreases up to pH around 4, and is relatively independent of the pH of the solution up to pH 10 [57]. If Fe(III) and Fe(II) are simultaneously present, Fe(II) will tend to coprecipitate with Fe(III) forming oxyhydroxides at pH values above 3 [58,59]. This explains the lack of reaction of toluene at pH 4 and 5 in the present work. The low variation of pH in the experiments at pH 3 of the present paper maintains a favorable acid pH condition, and it is an important result of the present work.

The use of pH 3 was also beneficial as it was found that the oxidation of toluene by the Fenton reagent with dissolved Fe(II) at a strong acid pH value (1.3) favors bibenzyl formation, whereas, at pH 3.6, the cresols predominate [50].

3.10. Toxicity of the products and discharge regulations

Regarding toxicity, Table A1 in the Appendix A (Section A3) indicates the LD_{50} for oral rat for toluene and its oxidation products. The values reveal that bibenzyl is the most toxic product after toluene. However, the results of the present work show that the oxidation products are formed at very low concentrations and during a short irradiation time (30 min).

On the other hand, the Argentine normative of ACUMAR (Matanza Riachuelo Basin Authority) established the permissible limits in discharge to storm drain for toluene in 1.36/17 mg L^{-1} [60]. The best toluene removal values obtained in the present work are in the range admitted by ACUMAR.

3.11. Advantages of the use of nZVI in the Fenton reactions for toluene oxidation

The use of nanoparticles compared with the homogeneous Fenton reaction with dissolved Fe(II) under the condition of this work presents some advantages: 1) using dissolved Fe(II), high concentrations of ferrous salts are needed, with the formation of a concomitant large amount of iron sludge; 2) with nZVI, a lower precipitation of iron hydroxides/oxides occurs because few iron ions are present in the aqueous phase; 3) a lower amount of the toxic bibenzyl compound is formed; 4) the separation of the catalyst after application is easy, while excess soluble Fe remains in solution when using Fe(II); 5) the catalyst can be reused without excessive manipulation; 6) the use of nZVI particles can be convenient for in situ applications.

4. Conclusions

Degradation of toluene (100 mg L^{-1}) under UVA irradiation in the presence of commercial nZVI at two concentrations (100 and 10 mg L^{-1}) and different H_2O_2 concentrations (25–400 mg L^{-1}) have been analyzed at pH 3. The highest removal of toluene was found with 100 mg L^{-1} nZVI and 400 mg L^{-1} H_2O_2 (18% toluene remaining in solution), although the degradation rate did not change very much with 100 and 200 mg L^{-1} of H_2O_2. At pH 4 and 5, no toluene removal was observed. The results have been compared with those of the homogeneous photo-Fenton reaction using Fe(II), although at lower Fe(II) concentrations (10 and 1 mg L^{-1}). The homogeneous reactions were faster than those with nZVI. In particular, 10 mg L^{-1} of Fe(II) with 400 mg L^{-1} H_2O_2 degraded 79% of toluene, while 100 mg L^{-1} of nZVI led to 65% degradation. This is due because dissolved Fe(II) is more available than Fe(0), which needs first to be oxidized to Fe(II) to start the photo-Fenton reaction. Experiments in the dark using 100 mg L^{-1} nZVI or 10 mg L^{-1} aqueous Fe(II) together with 200 mg L^{-1} H_2O_2 at pH 3 during 30 min showed a rather low toluene removal (<30%).

With both Fe(II) and nZVI, the main oxidation products were benzaldehyde, bibenzyl and lower concentrations of benzyl alcohol, *o*-cresol, and *p*-cresol. The quantity of byproducts depended greatly on the experimental conditions (especially on H_2O_2 concentration and nature of iron). With nZVI, the concentrations of benzaldehyde and bibenzyl were lower than with Fe(II) under similar concentrations.

The amount of Fe found in solution at the end of the experiments was comparatively lower in the experiments with nZVI compared with those that used Fe(II).

It was found that nZVI can be reused, maintaining the capacity of toluene degradation, an important advantage compared with the homogeneous reaction.

The use of nanoparticles compared with the use of dissolved Fe(II) is more advantageous because the precipitation of iron hydroxides/oxides can be avoided, a lower amount of the very toxic bibenzyl is formed, the separation of the catalyst after application is easy, and the nanoparticles can be reused.

CRediT authorship contribution statement

Clara Duca: Methodology, Investigation, Data curation, Formal analysis, Writing – original draft. **Horacio Bogo:** Methodology, Investigation, Data curation, Formal analysis, Writing – original draft. **Marta I. Litter:** Conceptualization, Methodology, Investigation, Funding acquisition, Writing – original draft, Writing – review & editing, Supervision. **Enrique San Román:** Conceptualization, Methodology, Investigation, Funding acquisition, Writing – original draft, Supervision.

Declaration of Competing Interest

The authors declare no conflict of interest.

Data availability

Data will be made available on request.

Acknowledgments

This work was financially supported by the P-UE 2020 IIIA-CONICET project of Argentina.

Appendix A. Supplementary data

Supplementary data to this article can be found online at https://doi.org/10.1016/j.catcom.2023.106767.

References

[1] M. Dehghani, E. Shahsavani, M. Farzadkia, M.J. Reza Samaei, Optimizing photo-Fenton like process for the removal of diesel fuel from the aqueous phase, J. Environ. Health Sci. 12 (2014) 87–93, https://doi.org/10.1186/2052-336X-12-87.

[2] A. Alva-Argáez, A.C. Kokossis, R. Smith, The design of water-using systems in petroleum refining using a water-pinch decomposition, Chem. Eng. J. 128 (2007) 33–46, https://doi.org/10.1016/j.cej.2006.10.001.

[3] W.F. Elmobarak, B.H. Hameed, F. Almomani, A.Z. Abdullah, A review on the treatment of petroleum refinery wastewater using advanced oxidation processes, Catalysts 11 (2021) 782, https://doi.org/10.3390/catal11070782.

[4] E.R. Lopes Tiburtius, P. Peralta-Zamora, A. Emmel, Treatment of gasoline-contaminated waters by advanced oxidation processes, J. Hazard. Mater. 126 (2005) 86–90, https://doi.org/10.1016/j.jhazmat.2005.06.003.

[5] J.J. Pignatello, E. Oliveros, A. MacKay, Advanced oxidation processes for organic contaminant destruction based on the Fenton reaction and related chemistry, Crit. Rev. Environ. Sci. Technol. 36 (2006) 1–84, https://doi.org/10.1080/10643380500326564.

[6] A.V. Vorontsov, Advancing Fenton and photo-Fenton water treatment through the catalyst design, J. Hazard. Mater. 372 (2019) 103–112, https://doi.org/10.1016/j.jhazmat.2018.04.033.

[7] M.I. Litter, Introduction to oxidative technologies of water treatment, in: J. Filip, T. Cajthaml, P. Najmanová, M. Černík, R. Zbořil (Eds.), Advanced Nano-Bio

Technologies for Water and Soil Treatment, Springer Cham, New York City, 2020, pp. 119–175, https://doi.org/10.1007/978-3-030-29840-1_7.
[8] M. Xu, C. Wu, Y. Zhou, Advancements in the Fenton process for wastewater treatment, in: C. Bustillo-Lecompte (Ed.), Advanced Oxidation Processes – Applications, Trends and Prospects, IntechOpen, 2020, https://doi.org/10.5772/intechopen.85681.
[9] M.I. Litter, M. Slodowicz, An overview on heterogeneous Fenton and photoFenton reactions using zerovalent iron materials, J. Adv. Oxid. Technol. 20 (2017), https://doi.org/10.1515/jaots-2016-0164, 2371–1175.
[10] P. Wardman, Reduction potentials of one-Electron couples involving free radicals in aqueous solution, J. Phys. Chem. Ref. Data Monogr. 18 (1989) 1637–1655, https://doi.org/10.1063/1.555843.
[11] H. Bataineh, O. Pestovsky, A. Bakac, pH-induced mechanistic changeover from hydroxyl radicals to iron(IV) in the Fenton reaction, Chem. Sci. 3 (2012) 1594–1599, https://doi.org/10.1039/C2SC20099F.
[12] S. Pang, J. Jiang, J. Ma, Oxidation of sulfoxides and arsenic(III) in corrosion of nanoscale zero valent iron by oxygen: evidence against ferryl ions (Fe(IV)) as active intermediates in Fenton reaction, Environ. Sci. Technol. 45 (2011) 307–312, https://doi.org/10.1021/es102401d.
[13] R. Ameta, A.K. Chohadia, A. Jain, P.B. Punjabi, Fenton and photo-Fenton processes, in: S. Ameta, R. Ameta (Eds.), Advanced Oxidation Processes for Wastewater Treatment: Emerging Green Chemical Technology, Academic Press, Cambridge, MA, 2018, pp. 49–86, https://doi.org/10.1016/B978-0-12-810499-6.00003-6.
[14] A.C. Coelho, A.V. Dezotti, M. Sant, G.L. Anna, Treatment of petroleum refinery sourwater by advanced oxidation processes, J. Hazard. Mater. 137 (2006) 178–184, https://doi.org/10.1016/j.jhazmat.2006.01.051.
[15] T.S.B.A. Manan, T. Khan, S. Sivapalan, H. Jusoh, N. Sapari, A. Sarwono, R. M. Ramli, S. Harimurti, S. Beddu, S.N. Sadon, N.L.M. Kamal, A. Malakahmad, Application of response surface methodology for the optimization of polycyclic aromatic hydrocarbons degradation from potable water using photo-Fenton oxidation process, Sci. Total Environ. 665 (2019) 196–212, https://doi.org/10.1016/j.scitotenv.2019.02.060.
[16] Y. Xue, S. Lu, X. Fu, V.K. Sharma, I. Mendoza-Sanchez, Z. Qiu, Q. Sui, Simultaneous removal of benzene, toluene, ethylbenzene, and xylene (BTEX) by CaO_2 based Fenton system: enhanced degradation by chelating agents, Chem. Eng. J. 331 (2018) 255–264, https://doi.org/10.1016/j.cej.2017.08.099.
[17] Y. Chen, C.J. Miller, T.D. Waite, Heterogeneous Fenton chemistry revisited: mechanistic insights from Ferrihydrite-mediated oxidation of Formate and oxalate, Environ. Sci. Technol. 55 (2021) 14414–14425, https://doi.org/10.1021/acs.est.1c00284.
[18] N. Thomas, D.D. Dionysiou, S.C. Pillai, Heterogeneous Fenton catalysts: a review of recent advances, J. Hazard. Mater. 404 (2021) 124082, https://doi.org/10.1016/j.jhazmat.2020.124082.
[19] G. Scaratti, T.G. Rauen, V.Z. Baldissarelli, H.J. José, R.D.F.P.M. Moreira, Residue-based iron oxide catalyst for the degradation of simulated petrochemical wastewater via heterogeneous photo-Fenton process, Environ. Technol. 1–9 (2017), https://doi.org/10.1080/09593330.2017.1361474.
[20] M.I. Litter, Future and perspectives of the use of Iron nanoparticles for water and soil remediation, in: M.I. Litter, N. Quici, M. Meichtry (Eds.), Iron Nanomaterials for Water and Soil Treatment, Pan Stanford, Singapore, 2018, pp. 308–316.
[21] M.I. Litter, A. Ahmad, Industrial Applications of Nanoparticles – A Prospective Overview, CRC Taylor & Francis Group, Boca Raton, FL, 2023. ISBN: 9781032024769.
[22] L.E. Lan, F.D. Reina, G.E. De Seta, J.M. Meichtry, M.I. Litter, Comparison between different technologies (zerovalent iron, coagulation-flocculation, adsorption) for arsenic treatment at high concentrations, Water 15 (2023) 1481, https://doi.org/10.3390/w15081481.
[23] S.R. Kanel, B. Manning, L. Charlet, H. Choi, Removal of arsenic(III) from groundwater by nanoscale zero-valent iron, Environ. Sci. Technol. 39 (2005) 1291–1298, https://doi.org/10.1021/es048991u.
[24] J.H. Merz, W.A. Waters, The oxidation of aromatic compounds by means of the free hydroxyl radical, J. Chem. Soc. (1949) 2427–2433, https://doi.org/10.1039/jr9490002427.
[25] C. Walling, R.A. Johnson, Fenton's reagent. V. Hydroxylation and side-chain cleavage of aromatics, J. Amer. Chem. Soc. 97 (1975) 363–367, https://doi.org/10.1021/ja00835a024.
[26] S.G. Huling, S. Hwang, D. Fine, S. Ko, Fenton-like initiation of a toluene transformation mechanism, Water Res. 45 (2011) 5334–5342, https://doi.org/10.1016/j.watres.2011.08.001.
[27] M. Alizadeh Fard, A. Torabian, G.R.N. Bidhendi, B. Aminzadeh, Fenton and photo-fenton oxidation of petroleum aromatic hydrocarbons using nanoscale zero-valent Iron, J. Environ. Eng. 139 (2013) 966–974, https://doi.org/10.1061/(ASCE)EE.1943-7870.0000705.
[28] E.B. Sandell, Colorimetric Determination of Traces of Metals, Interscience Publishers, New York, 1950.
[29] Y. Liu, S.A. Majetich, R.D. Tilton, D.S. Sholl, G.V. Lowry, TCE dechlorination rates, pathways, and efficiency of nanoscale iron particles with different properties, Environ. Sci. Technol. 39 (2005) 1338–1345, https://doi.org/10.1021/es049195r.
[30] http://nanoiron.cz/en/products/zero-valent-iron-nanoparticles/nanofer-star.
[31] L. Cancelada, J.M. Meichtry, H. Destaillats, M.I. Litter, Heterogeneous sonoFenton removal of Cr(VI) in the presence of organic additives, in preparation.
[32] A.S. Mahmoud, M.K. Mostafa, S.A. Abdel-Gawad, Artificial intelligence for the removal of benzene, toluene, ethyl benzene and xylene (BTEX) from aqueous solutions using iron nanoparticles, Water Sci. Technol. Water Supply 18.5 (2018), https://doi.org/10.2166/ws.2017.225.
[33] V. Tanboonchuy, J.C. Hsu, N. Grisdanurak, C.H. Liao, Impact of selected solution factors on arsenate and arsenite removal by nanoiron particles, Environ. Sci. Pollut. Res. Int. 18 (2011) 857–864, https://doi.org/10.1007/s11356-011-0442-3.
[34] C. Noubactep, Comment on pH dependence of Fenton reagent generation and As (III) oxidation and removal by corrosion of zero valent iron in aerated water, Environ. Sci. Technol. 43 (2009) 233, https://doi.org/10.1021/es802563j.
[35] G. Ona-Nguema, G. Morin, Y. Wang, A.L. Foster, F. Juillot, G. Calas, G.E. Brown Jr., XANES evidence for rapid arsenic(III) oxidation at magnetite and ferrihydrite surfaces by dissolved O_2 via Fe^{2+}-mediated reactions, Environ. Sci. Technol. 44 (2010) 5416–5422, https://doi.org/10.1021/es1000616.
[36] M.E. Morgada, I.K. Levy, V. Salomone, S.S. Farías, G. López, M.I. Litter, Catal. Today 143 (2009) 261–268, https://doi.org/10.1016/j.cattod.2008.09.038.
[37] D.C. Pabón Reyes, E.B. Halac, M.I. Litter, As(III) removal of aqueous solutions using zerovalent iron nanoparticles: the role of the UVA-Vis irradiation wavelength, J. Photochem. Photobiol. A 443 (2023) 114846, https://doi.org/10.1016/j.jphotochem.2023.114846.
[38] H. Christensen, K. Sehested, H. Corfitzen, Reactions of hydroxyl radicals with hydrogen peroxide at ambient and elevated temperatures, J. Phys. Chem. 86 (1982) 1588–1590, https://doi.org/10.1021/j100206a023.
[39] World Health Organization, Guidelines for drinking-water quality: fourth edition incorporating the first addendum, ISBN 978-92-4-154995-0 -water.
[40] H. Dong, F. Zhao, Q. He, Y. Xie, Y. Zeng, L. Zhang, L. Tang, G. Zeng, Physicochemical transformation of carboxymethyl cellulose-coated zero-valent iron nanoparticles (nZVI) in simulated groundwater under anaerobic conditions, Sep. Purif. Technol. 175 (2017) 376–383, https://doi.org/10.1016/j.seppur.2016.11.053.
[41] B.A. Balko, P.G. Tratnyek, Photoeffects on the reduction of carbon tetrachloride by zero-valent Iron, J. Phys. Chem. B 102 (1998) 1459–1465, https://doi.org/10.1021/jp973113m.
[42] V.N. Montesinos, N. Quici, M.I. Litter, Visible light enhanced Cr(VI) removal from aqueous solution by nanoparticulated zerovalent iron, Catal. Commun. 46 (2014) 57–60, https://doi.org/10.1016/j.catcom.2013.11.024.
[43] M. Fujihira, Y. Satoh, T. Osa, Heterogeneous photocatalytic oxidation of aromatic compounds on semiconductor materials: the photo-Fenton type reaction, Chem. Lett. 10 (1981) 1053–1056, https://doi.org/10.1246/cl.1981.1053.
[44] M. Fujihira, Y. Satoh, T. Osa, Heterogeneous photocatalytic reactions on semiconductor materials. III. Effect of pH and Cu^{2+} ions on the photo-Fenton type reaction, Bull. Chem. Soc. Jpn. 55 (1982) 666–671, https://doi.org/10.1246/bcsj.55.666.
[45] Y. Zhang, N. Zhang, T. Wang, H. Huang, Y. Chen, Z. Li, Z. Zou, Heterogeneous degradation of organic contaminants in the photo-Fenton reaction employing pure cubic β-Fe_2O_3, Appl. Catal. B 245 (2019) 410–419, https://doi.org/10.1016/j.apcatb.2019.01.003.
[46] R. Chen, J.J. Pignatello, Role of quinone intermediates as electron shuttles in Fenton and photoassisted Fenton oxidations of aromatic compounds, Environ. Sci. Technol. 31 (1997) 2399–2406, https://doi.org/10.1021/es9610646.
[47] G.V. Buxton, C. Greenstock, W.P. Hellman, A.B. Ross, Critical review of rate constants for reactions of hydrated electrons, hydrogen atoms and hydroxyl radicals ($^{\bullet}OH/^{\bullet}O^{-}$) in aqueous solution, J. Phys. Chem. Ref. Data Monogr. 17 (1988) 513–886, https://doi.org/10.1063/1.555805.
[48] H.C. Christensen, K. Sehested, E.J. Hart, Formation of benzyl radicals by pulse radiolysis of toluene in aqueous solutions, J. Phys. Chem. 77 (1973) 983–987, https://doi.org/10.1021/j100627a003.
[49] L.M. Dorfman, I.A. Taub, D.A. Harter, Rate constants for the reaction of the hydroxyl radical with aromatic molecules, J. Chem. Phys. 41 (1964) 2954–2955, https://doi.org/10.1063/1.1726387.
[50] C.R.E. Jefcoate, J.R. Lindsay Smith, R.O.C. Norman, Hydroxylation. Part IV. oxidation of some benzenoid compounds by Fenton's reagent and the ultraviolet irradiation of hydrogen peroxide, J. Chem. Soc. B (1969) 1013–1018, https://doi.org/10.1039/J29690001013.
[51] J.R.L. Smith, R.O.C. Norman, Hydroxylation. Part I. The oxidation of benzene and toluene by Fenton's reagent, J. Chem. Soc. (1963) 2897–2905, https://doi.org/10.1039/JR9630002897.
[52] J.P. Hage, A. Llobet, D.T. Sawyer, Aromatic hydroxylation by Fenton reagents {reactive intermediate[Lx+FeIIOOH(BH+)], not free hydroxyl radical ($HO^{\bullet}$)}, Bioorg. Med. Chem. 3 (1995) 1383–1388, https://doi.org/10.1016/0968-0896(95)00123-x.
[53] H.C. Christensen, R. Gustafsson, Radiation of aqueous toluene solutions, Acta Chem. Scand. 26 (1972) 937–946, https://doi.org/10.3891/acta.chem.scand.26-0937.
[54] M. Altarawneh, A.A.H. Al-Muhtaseb, B.Z. Dlugogorski, E.M. Kennedy, J.C. Mackie, Rate constants for hydrogen abstraction reactions by the hydroperoxyl radical from methanol, ethenol, acetaldehyde, toluene, and phenol, J. Comput. Chem. 32 (2011) 1725–1733, https://doi.org/10.1002/jcc.21756.
[55] K. Choi, S. Bae, W. Lee, Degradation of off-gas toluene in continuous pyrite Fenton system, J. Hazard. Mater. 280 (2014) 31–37, https://doi.org/10.1016/j.jhazmat.2014.07.054.
[56] M.I. Litter, Introduction to photochemical advanced oxidation processes for water treatment, in: Environmental Photochemistry Part II, Springer, Berlin, Heidelberg, 2005, pp. 325–366.
[57] U.S. Dept. of Energy, DOE Fundamentals Handbook Chemistry vol. 1, U.S. Dept. of Energy, Washington, DC, 1993.

[58] C.R. Keenan, D.L. Sedlak, Factors affecting the yield of oxidants from the reaction of nanoparticulate zero-valent iron and oxygen, Environ. Sci. Technol. 42 (2008) 1262–1267, https://doi.org/10.1021/es7025664.
[59] C.R. Keenan, D.L. Sedlak, Ligand-enhanced reactive oxidant generation by Nanoparticulate zero-valent Iron and oxygen, Environ. Sci. Technol. 42 (2008) 6936–6941, https://doi.org/10.1021/es801438f.
[60] N° 5270-7/12/2017 Separata del Boletín Oficial de la Ciudad de Buenos Aires N° 756 ANEXO - RESOLUCIÓN N° 471/APRA/17 ANEXO I: Límites permisibles de vertido.